

How asymmetric chirality and chain density affect chain stiffness of polymer melts

Ran Chen^a, Chuanfu Luo^{a,b,*}

^a State Key Laboratory of Polymer Physics and Chemistry, Changchun Institute of Applied Chemistry, Chinese Academy of Sciences, Changchun, 130022, PR China

^b University of Science and Technology of China, Hefei, PR China

ARTICLE INFO

MSC:
10-17

Keywords:
Simulation
Stiffness
Temperature coefficient

ABSTRACT

Chain stiffness plays a critical role in influencing the thermodynamic and dynamic properties of polymers. Here, all-atom molecular dynamics simulations are employed to study the effects of chain tacticity and temperature on polymer stiffness. Our results show that local stiffness is enhanced by introducing an asymmetric stereochemical unit with opposite chirality joined by all-*trans* series on polymer chains. The free energy landscape of adjacent dihedral pairs can explain the various chain stiffness of polymer chain with different tacticities. In literature, the temperature dependence of chain stiffness measured by small-angle neutron scattering (SANS)-based experiments contradicts with rotational isomeric state (RIS) predictions and recent single chain simulation results. Our results show that chain stiffness of isotactic PP and PB-1 melt is almost temperature independent, which is consistent with SANS-based measurements. By considering the chain density of polymer melt which is ignored by original RIS theory and single-chain simulations, we point that RIS theory and SANS-based experiments can be harmonic, but the chain density must be explicitly considered for polymer melt.

1. Introduction

Chain conformation is one of the crucial concepts in the field of polymer physics since it lays the molecular foundation of all physical properties of polymer materials. Most of polymers adopt a substantial number of chain conformations as a result of rotation around single bonds along chain backbone. There are several “preferred” rotational (dihedral) angles for each polymer, such as *trans* and *gauche* states. Simple transitions between available isomeric states of chain conformations give rise to chain stiffness which will also change the thermodynamic and dynamic properties of polymers as a consequence [1]. Thus, understanding the impact of tacticity on the chain stiffness of polymers at the molecular level is of significant importance in the scientific field and the technological applications of the materials.

Considerable efforts have been made to explore chain stiffness of polymers, which is usually expressed by Flory’s characteristic ratio, C_n , or through persistence length, l_p . Experimentally, the chain stiffness under the unperturbed state can be evaluated by the technique of small-angle neutron scattering (SANS) [2–6] and intrinsic viscosity measurements in Θ conditions [7–9]. In theoretical treatments, the development of Rotational Isomeric State (RIS) model has made a

breakthrough in predicting the chain stiffness of polymer systems [10–15]. With the improvement of computing ability, Monte Carlo (MC) simulations [16–18] and molecular dynamics (MD) simulations [19–22] have been performed to extract the chain dimensions and stiffness of various polymers. The combination of MC simulations and RIS theory has been proposed and implemented for single polymer chains [23,24].

Tacticity plays an important role in the properties of polymers, such as dynamical [19,20] and rheological properties [25–28], which has been extensively studied in the literature. Polypropylene (PP) is a typical kind of polymers with high regulation of various stereoregularity, such as isotactic polypropylene (*i*PP), syndiotactic polypropylene (*s*PP), and atactic polypropylene (*a*PP). The comparison between PP with different tacticity has been extensively studied. [25–33]. *s*PP shows excellent elastic properties compared to *i*PP [29–31]. The more striking difference lies in chain dimensions and rheological behavior in melt state [27,28]. For instance, Jones and coworkers [28] found that *s*PP exhibits dramatically larger chain dimensions than *i*PP. Eckstein *et al* [25,26] showed that the plateau modulus of *s*PP with high stereoregularity is greatly larger than those of *i*PP and *a*PP, which has been further confirmed recently [32]. The probable reason for this phenomenon is that *trans* conformation dominates in the *s*PP melts.

* Corresponding author at: State Key Laboratory of Polymer Physics and Chemistry, Changchun Institute of Applied Chemistry, Chinese Academy of Sciences, Changchun, 130022, PR China.

E-mail addresses: ranchen@ciac.ac.cn (R. Chen), luocf@ciac.ac.cn (C. Luo).

<https://doi.org/10.1016/j.commsci.2021.111071>

Received 24 August 2021; Received in revised form 15 November 2021; Accepted 17 November 2021

Available online 8 December 2021

0927-0256/© 2021 Elsevier B.V. All rights reserved.

Moreover, MD simulations [33] have been reported to study the effect of tacticity on the dynamics of PP chains in melt state.

Tacticity has a significant influence on the chain stiffness of polymers, as it mainly affects the distributions of dihedral angles along chain backbone. Relevant results for PP have been reported in both experiments [27,28] and theoretical calculations [12–15,34]. Antoniadis and coworkers [19,20] applied MD simulations to the system of PP with different tacticities and found that the difference of transition rates between different isomeric states is accountable for the tacticity effect on the segmental dynamics. A recent systematic study of single chain by MC simulations [16] investigated the effect of tacticity on the stiffness of a PP chain under the unperturbed state, where the Flory's characteristic ratio exhibited a nonmonotonic dependence on the tacticity expressed by fractions of *meso* dyads. Moreover, the hybrid particle-field molecular dynamics was proposed to describe conformational differences of polymer chains as a function of tacticity [22]. It was also reported for polybutene-1 (PB-1) that the stereoregularity plays a key role in determining chain stiffness. [35] Despite tremendous efforts, how the tacticity influences the chain stiffness and conformations at the fundamental molecular scale remains to be better understood. We must emphasize that most of the previous theoretical treatments and simulations in literature are based on single-chain system and their conclusion might need further correction for polymer melt.

It is notable that there is a wide discrepancy of the temperature coefficient ($\kappa = d \ln \langle R^2 \rangle / dT = d \ln C_n / dT$) of chain dimensions and stiffness in actual results from different methods. For example, the majority of RIS predictions [14,15,34,36–38] and the measurements from θ -condition [39–41] on PP yield large negative values of κ . A recent MC simulation [17] also gives a negative value of κ (-0.56 K^{-1}) due to the entropic elasticity. However, the SANS-based melt results [3,5] lead to a contradicted conclusion that κ is almost zero. A similar phenomenon is found for PB-1 [5,42]. The κ value of PB-1 from the melt calculated using SANS results yields a small positive value about $0.4 \times 10^{-3} \text{ K}^{-1}$ while the intrinsic viscosity measurements show negative values. The contradiction between SANS-based measurements and RIS predictions and θ -solution evaluations is also found for polystyrene [43–45]. It is supposed that the diverse results are caused by the correlation effects in the melt [5], which is neglected in either θ -solution measurements or RIS predictions. The fact that there is a good agreement among θ -condition results [46], RIS predictions [36] and SANS-based melt results [47] on κ value of polyethylene (without side groups) further confirms this supposition. But this interpretation underlying the obvious contradiction is still not clarified. The dependence of chain stiffness on temperature is important because it is related to the polymer properties at different temperatures during processing stages. Thus, it is of interest to evaluate the temperature dependence of polymer chain stiffness at molecular scale.

In the present study, we employ all-atom MD simulations to explore the role of tacticity and temperature on the chain stiffness of polymer in the melt. Specifically, PP and PB-1 with different tacticities are employed to explore the effect of tacticity on chain stiffness. Meanwhile, MD simulations of *i*PP, *i*PB-1, and PE at different temperatures are performed to estimate the temperature dependence of chain stiffness. By evaluating the local molecular stiffness, quantified by Flory's characteristic ratio and local persistence length, we can obtain insights into the mechanism in action of tacticity. The results of the current simulations highlight how tacticity influences the chain stiffness of polymer melt, which will be beneficial for the design of polymer materials and predictions of physical properties. Furthermore, we point out that original RIS theory and single-chain simulations cannot make a correct prediction of chain stiffness for polymer melt, as the density effect and the relative thermal expansion is not considered.

2. Methods

2.1. System studied

The systems we studied are a series of PP and PB-1 chains with various probabilities (fractions) of *meso* dyads, P_m . In particular, polymer chains with $P_m = 1.0$ and 0.0 correspond to isotactic and syndiotactic polymers, respectively. Several kinds of stereodeficient *i*PP (termed as *st-i*PP $P_m 0.71$, *st-i*PP $P_m 0.88$, *st-i*PP-block, *st-i*PP-dot) and *i*PB-1 (termed as *st-i*PB-dot) chains were studied. The schematic representations of polymer chains studied are depicted in Fig. 1. For a clearer view, the planar zigzag conformation is used and the side groups are displayed on both sides of the chain plane. The stereochemical sequence of each chain could also be illustrated by a color strap shown under the schematic representation in Fig. 1. All *meso* and *racemo* sequences are Bernoullian. All chains are arranged in head-to-tail sequence, where monomer inversion is not allowed. The chains are absolutely identical in each system; the *meso* and *racemo* sequences are exactly the same which is different from the previous paper. [16] The bulk system in this work contains 50 chains with 50 repeat units each chain, corresponding to a simulation box of 7500 carbon and 15100 hydrogen atoms for PP, and 10000 carbon and 20100 hydrogen atoms for PB-1. To investigate the temperature dependence of the chain stiffness of polymers, larger systems of PE, *i*PP, and *i*PB-1 are generated, consisting 100 chains with 100 repeat units.

2.2. Overview of MD simulations

All MD simulations are carried out using GROMACS (version 4.5) software package [48] with the all-atom model of OPLS force field (OPLS-AA) [49,50], which has been widely applied in previous studies. The interactions between atoms contain both bonded (bond, angle, and dihedral) and nonbonded (van der Waals and Coulomb) potentials. A cut-off distance of $r_c = 1.2 \text{ nm}$ is implemented in the Lennard-Jones potential and the Coulomb potential. The leap-frog algorithm with a time step $dt = 2 \text{ fs}$ for the dynamic integration is used in all MD simulations and periodic boundary conditions are applied in all directions. The *v-rescale* thermostat (velocity rescaling with a stochastic term) and Berendsen barostat are used to control the temperature and the pressure of the system. In our simulations, the initial configurations of polymer chains are first minimized by the steepest descent algorithm and melted at 600 K. The melt system is first compressed at 600 K and then equilibrated at a fixed temperature (500 K, 550 K, 600 K, or 650 K) under an isothermal-isobaric (NPT) ensemble with the pressure of 1 bar for at least 6 ns until the density of system maintains almost unchanged and the auto-correlation of end-to-end vector reaches 0.1. All the chosen temperatures are much higher than the glass transition temperature, and the system is surely in melt state at these temperatures. Afterward, the production run is performed under the canonical ensemble (NVT) at the corresponding temperatures for 300 ns – 870 ns.

3. Results and discussion

3.1. Effect of asymmetric tacticity on chain stiffness of polymers

To quantify the chain stiffness of polymers, we first calculate the modified local persistence length $l_p^{(k)}$, which is defined as [51–53]:

$$l_p^{(k)} = \left\langle \frac{\vec{r}_k}{|\vec{r}_k|} \cdot \vec{R} \right\rangle \quad (1)$$

where \vec{R} is the end-to-end distance vector of each chain and \vec{r}_k is the unit vector of the k th bond along chain backbone. $\langle \dots \rangle$ denotes average over all chains. Fig. 2 shows the modified local persistence length $l_p^{(k)}$ versus k at 600 K for PP and PB-1 chains, respectively. The local stiffness of *s*PP chain is much larger than *i*PP chain, consistent with previous experimental and theoretical studies. [16,25,26,28,32] PB-1 shows the

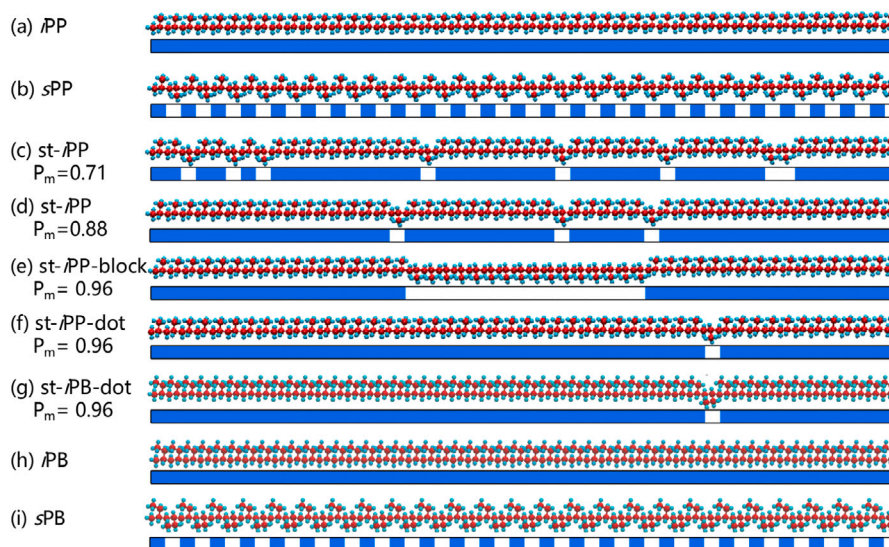


Fig. 1. Schematic all-atom and strapped representations of different polymer chains displayed with different tacticity in the zigzag conformation. The big red and the small cyan spheres represent C and H atoms, respectively. The stereochemical sequence of each chain is simplified and illustrated by a color strap shown under the corresponding schematic representation. The blue represents the repeat units with side groups above the zigzag plane and the white describes the ones under it.

same tendency with PP, which means that $sPB-1$ is stiffer than $iPB-1$. It can be observed that $l_p^{(k)}$ depends strongly on k near chain ends for all cases which we will discuss later. The values of $l_p^{(k)}$ reach a plateau value in the middle range of k for isotactic and syndiotactic polymers. However, it is interesting that there are some peaks on the basis of plateau values where *racemo* dyads are introduced for *st-iPP* and *st-iPB-1* chains. This indicates that the introduction of *racemo* dyads enhances the local chain stiffness. We can notice that a typical peak has been split into two little tips on the curve of $l_p^{(k)}$, and there is a concavity between the two tips. The exceptions on the curve of *st-iPP* with $p_m = 0.71$ near $k = 15$ and 86 are caused by the overlap of a few of neighboring peaks. We will discuss this characteristic later. It should be noted that when an ensemble of chains with various meso-*racemo* dyad sequences but all having the same percentage of meso dyads p_m is used, no peaks will appear at the plot of average $l_p^{(k)}$ versus k . We have performed additional simulations for *st-iPP-dot* system with randomly distributed meso-*racemo* dyad positions. Fig. S.2 presents the modified local persistence length $l_p^{(k)}$ versus k at $600K$ for the whole system and for a specific chain. The $l_p^{(k)}$ plot for the randomly distributed *st-iPP-dot* system shows no obvious peaks either, but peaks due to local enhanced chain stiffness can be seen considering only one chain in the system.

This phenomenon of enhanced chain stiffness raises the question that how *racemo* dyads affect the local molecular stiffness of polymers. We speculate that a large conformational change happens at the interfaces of two different stereochemical sequences and leads to a sudden increase of local stiffness. Thus, we take PP systems as examples to evaluate the relationship between chain conformations and chain stiffness. Fig. 3 shows the time-index space by means of dihedrals for a typical chain of *iPP*, *sPP*, and *st-iPP-dot*. The specially selected *st-iPP-dot* introduces one monomer with syndiotacticity in *iPP* chain, introducing two *racemo* dyads. It is taken as a model system to explore the physical explanation of the enhanced local stiffness, which is shown in the right panel of Fig. 3. The alternation of green and red or blue stripes represent helical segments (*trans-gauche* states), and the green stripes exhibit the sustained *trans* state. There are certain amounts of short helical segments in the *iPP* or *sPP* melts. It is worth noting that there is a green stripe (*trans-trans* states) where *racemo* dyads stay throughout the whole simulation time for *st-iPP-dot*, as seen in Fig. 3(c). This indicates that the probability of *trans* state is much larger in the polymer chain where *racemo* dyads are introduced than that at other positions. The sustained *trans* state means an increased

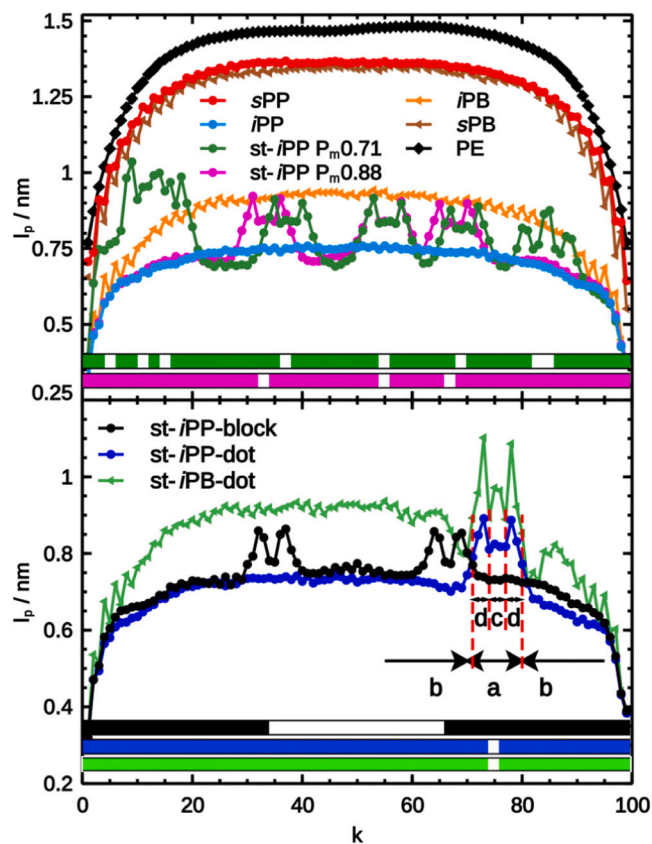


Fig. 2. Modified local persistence length $l_p^{(k)}$ versus k at $600K$ for polymers studied. The strapped stereochemical sequence is illustrated by different colors for clarity. The bottom panel displays the modified local persistence length of three stereodeficient polymer chains, named by *st-iPP-block*, *st-iPP-dot*, and *st-iPB-dot*, with same P_m value of 0.96 but of different stereochemical sequences. The areas of peak, non-peak, central part and marginal part of the peak are marked by "a", "b", "c", "d", which will be discussed in Fig. 4.

free energy barrier of rotation and makes a valuable contribution to enhanced local stiffness.

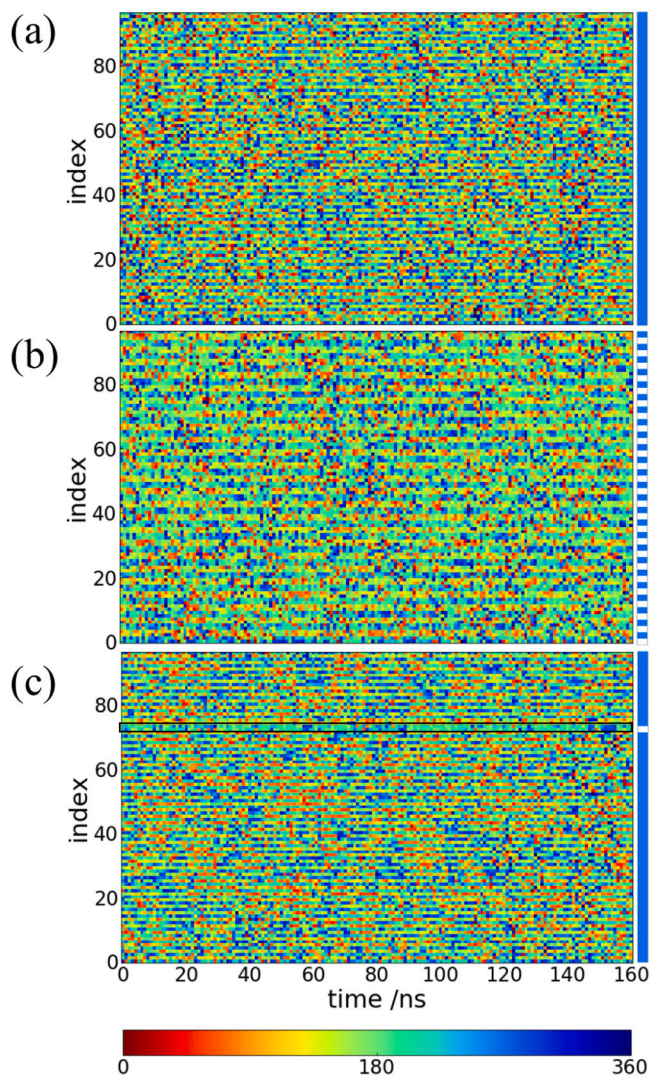


Fig. 3. Time-index space by means of dihedral for a typical chain of (a) *i*PP, (b) *s*PP, and (c) *st-i*PP-dot. The strapped representations of corresponding chains are shown on the right. The green strip is highlighted by the black rectangle box. The color bar is shown at the bottom.

To have a better understanding of the influence of the chain conformations on the stiffness of the chain where *racemo* dyads are introduced, we plot the equivalent free energy landscape of adjoint dihedral pairs (Φ - Ψ plot) for the *st-i*PP-dot chains at different bond index ranges in Fig. 4. The equivalent free energy landscape, $F(\Phi, \Psi)$, is calculated by the inverse Boltzmann formula:

$$F(\Phi, \Psi) = -k_B T \ln P(\Phi, \Psi) \quad (2)$$

where k_B is the Boltzmann constant and T is the temperature. $P(\Phi, \Psi)$ is the probability of adjoining (Φ, Ψ) pairs found in simulations. Fig. 4(a) and (b) show the equivalent free energy landscape of adjacent dihedral pairs at the bond index range corresponding to the peak and non-peak in the $l_p^{(k)}$ curve shown in Fig. 2. As expected, there are large quantities of *trans-trans* states (the strong dark and red points at the center) besides helical conformations at the peak range in comparison with the non-peak range where the *trans-gauche* states are dominating. This indicates that large quantity of *trans-trans* states contributes to the enhanced chain stiffness, which is consistent with the observation in Fig. 3. The bond index range at the peak is further divided into the central part and the marginal part, and the corresponding equivalent free energy landscape of adjacent dihedral pairs are displayed in

Fig. 4(c) and (d), respectively. It can be observed that the *trans-trans* states mainly exist at the center of the peak while the *trans-gauche* states (blocks of helical conformations) appear at the marginal part.

To facilitate a better insight into the conformational distribution near the introduced *racemo* dyads on polymer chain, we compare the corresponding equivalent free energy landscape of dihedral pairs between adjacent bonds of *st-i*PP-dot, as illustrated in Fig. 5. For clarity, a schematic representation of chain configuration in the planar zigzag conformation is described in the middle of Fig. 5. Side groups of *st-i*PP-dot at the opposite sides of the chain plane are denoted as “black” and “striped”. The “striped” one refers to the monomeric unit of different tacticity introduced into the isotactic chain. The equivalent free energy landscapes between two consecutive backbone bonds are specified. We take the “striped” side group as the chain segment center, and analyze the dihedral pairs from this center to both directions. As shown in Fig. 5(c), (g), and (h), conformational distributions of dyads reveal a preference for *trans-trans* conformers within two backbone bonds from the center. This observation is consistent with the previous study [20] that distributions of pairs of successive torsion angle prefer *trans-trans* conformation for *s*PP. Continuously away from the center, it is found that portions of bond pairs stay in helical conformations (*trans-gauche* states) of opposite chirality as shown in Fig. 5(b) and (d). This observation has been confirmed in published studies [54,55], which showed that the conformation of *s*PP chains in melt state is expected to exhibit short sequences of helices of opposite chirality separated by joints (long sequences of consecutive *trans* state) at the low cost of conformational energy. Fig. 5(a), (e), (f), and (i) show the equivalent free energy landscape of bond pairs corresponding to the plateau value of persistence length $l_p^{(k)}$ as shown in Fig. 2. We can observe that there is a small quantity of *trans-gauche* sequence. The all-*trans* sequences and the connected helical sequences along the chain contribute to an increase in chain stiffness. The all-*trans* sequences correspond to the concavity of the peak, while the connected helical sequences correspond to the little tips of the peak of $l_p^{(k)}$ as shown in Fig. 2.

The significant impact of chain tacticity on the molecular stiffness of PP chains has been illustrated in our simulations. It shows that the local persistence length $l_p^{(k)}$ appears to be strongly increased at the chain positions where repeat units with different stereoregularity are introduced. From the view of chain conformations and free energy landscape of adjacent dihedral pairs, we have attempted to provide a physical meaning and uncover the origin of enhanced chain stiffness. The results show that special conformational sequences, which are helical conformations with asymmetric chirality joined by all-*trans* series, prevail where variations in stereoregularity occur. Previous studies based on the RIS model reported that such conformational sequences have a low cost of conformational energy. [55] It has been reported that the dependence of the characteristic ratio, C_n , on tacticity, P_m , is not monotonic but exhibits a minimum as tacticity increases, which is caused by two competing mechanisms. [16] As P_m increases, all-*trans* sequences become shorter, which tends to decrease the chain stiffness, while at the same time more lengthy helical conformations appear, which results in the increase of chain stiffness.

3.2. Effect of chain density and temperature on chain stiffness of polymer melt

In this section, the temperature dependence of the chain stiffness of polymers is investigated for PE, *i*PP, and *i*PB-1 with 100 repeat units by evaluating the Flory’s characteristic ratio C_n and the modified local persistence length $l_p^{(k)}$ at different temperatures. The selected temperatures are 550, 600, 650 K for PE system, 500, 600, 650 K for *i*PP, and 500, 550, 650 K for *i*PB, respectively. These temperatures are represented by T_{low} , T_{mid} and T_{high} in an increasing order. Fig. 6(a) plots the Flory’s characteristic ratio C_n of PE, *i*PP and *i*PB versus the length of chain backbone in form of bond number n at different temperatures.

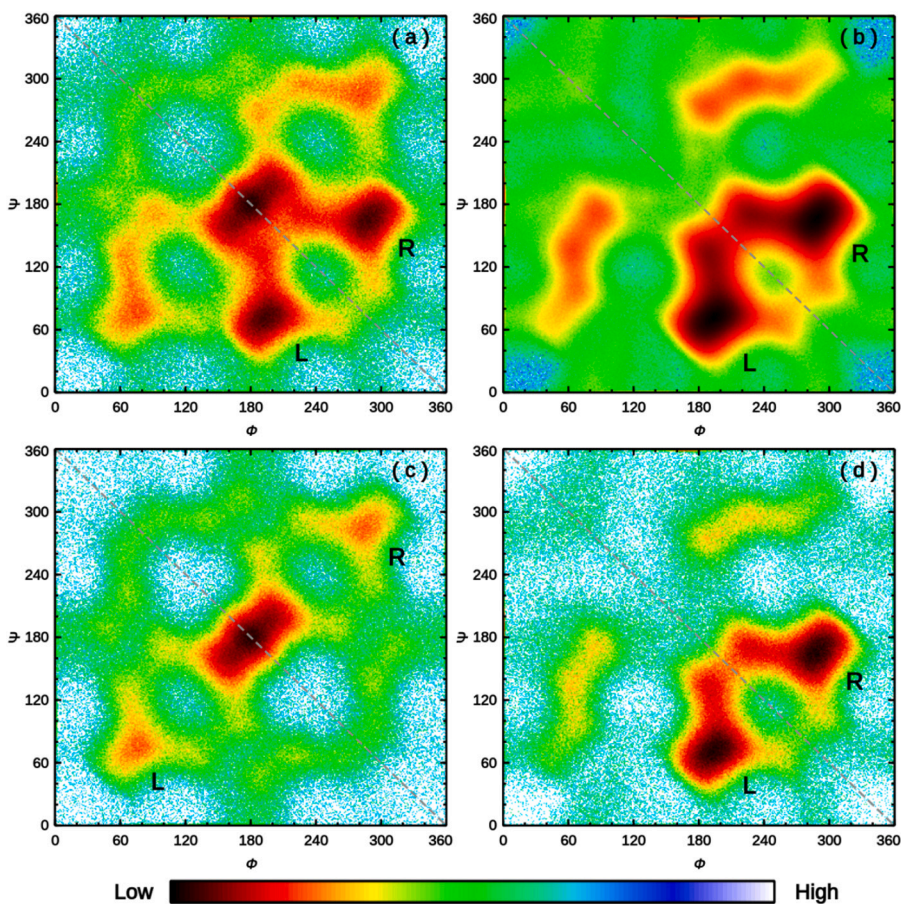


Fig. 4. Equivalent free energy landscape of adjacent dihedral pairs at different bond index ranges: (a) peak, (b) non-peak, (c) central part and (d) marginal part of the peak in the $l_p^{(k)}$ curve shown in Fig. 2. The left- and right-handed helices are divided by the diagonal and are represented by the “L” and “R” letters.

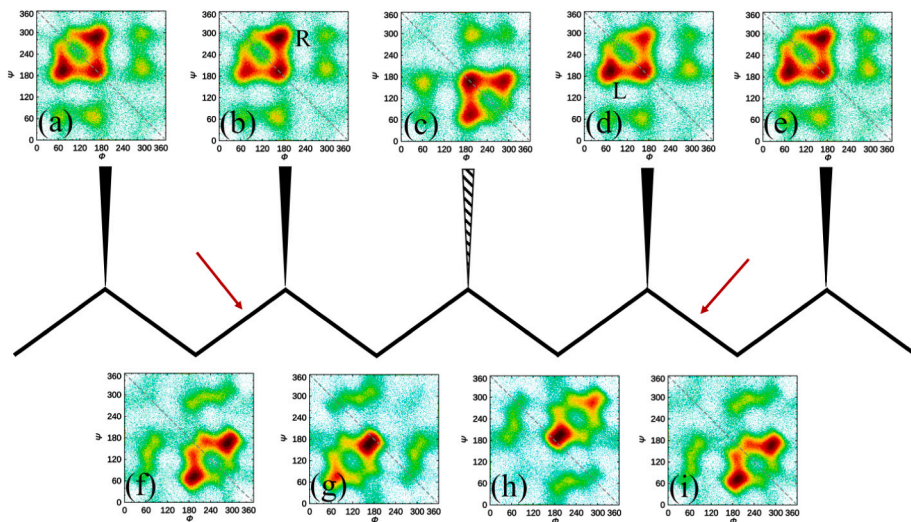


Fig. 5. Equivalent free energy landscape between adjacent bonds of st-*i*PP-dot. The two red arrows mark the two little tip values of $l_p^{(k)}$ curve shown in Fig. 2.

It can be observed that C_n reaches a plateau value at certain values of n . The plateau value of PE decreases with increasing temperature. However, it does not show much difference between *i*PP and *i*PB-1.

Fig. 6(b) shows the modified local persistence length $l_p^{(k)}$ of PE, *i*PP and *i*PB-1 at different temperatures. The dependence of $l_p^{(k)}$ on k can be well described by an approximation, proposed by Schäfer, [56,57]

which are plotted using dashed lines:

$$l_p^{(k)} / l = \alpha [k(N_b - k) / N_b]^{2\nu - 1} \tag{3}$$

where α is a (nonuniversal) constant, l is the bond length, and N_b is the total number of monomers. ν is the exponent characterizing chain linear dimensions in good solvents, where $\langle R^2 \rangle \propto N_b^{2\nu}$. It shows that there is some deviation for our results from Eq. (3). We attribute

such deviations to two factors: From one point, the suitably applied situation of Eq. (3) is a single chain in solvent without interchain correlations, but the condition in our results is polymers in the melt state. From the other point, the definition of Eq. (3) decides that there is a convex variation with the maximum around the right middle, which contradicts with the flat plateau in the chain interior in our results. Similarly to C_n , there is no obvious temperature dependence of $l_p^{(k)}$ for *i*PP or *i*PB-1.

As mentioned above, RIS model and previously reported single-chain simulations ignored the multi-chain effect, i.e., the effect of chain density and thermal expansion. However, in our all-atom simulations of polymer melt, it is found that thermal expansion and the chain density of PE, *i*PP and *i*PB-1 cannot be ignored. For a given pressure of 1 bar, the densities of PE, *i*PP and *i*PB-1 are slightly different. However, the chain densities are more different due to the sizes of side-groups of *i*PP and *i*PB-1. Flory states that polymer conformations in a melt behave statistically random-walks as Gaussian chains, and the results of end-to-end distance and radius of gyration in our simulations further support it. There, in order to exclude the thermal expansion effect, we scale $l_p^{(k)}$ at different temperatures by the same volume of every system, and introduce the normalized local persistence length, l_p^* , for *i*PP and *i*PB-1, which is defined as:

$$l_p^* = l_p^{(k)} \frac{v_0^{1/3}}{v^{1/3}} \quad (4)$$

Where, v and v_0 are the volume of considered polymer melt and the reference (1000 nm^3). In this way, the values of $l_p^{(k)}$ and l_p^* of our simulation results can be compared to the experimental SANS data and calculated RIS data, respectively.

Fig. 6(c) shows that the normalized persistence length l_p^* of *i*PP decreases obviously with increasing temperature, which is qualitatively consistent with RIS results [14,15,34,36–38]. These results indicate a negative value of κ for *i*PP. While the molecular stiffness of *i*PP, described by Flory's characteristic ratio C_n and modified local persistence length $l_p^{(k)}$, does not show a temperature-dependent relationship, which is in agreement with experimental SANS results [3,5]. The compensation of thermal expansion causes the negative value of κ to be around zero for *i*PP. We hereby conclude that the chain density and thermal expansion of chain dimensions leads to the contradicted results between SANS-based experiments and those from RIS prediction and single-chain simulation. The temperature dependence of melt density is involved by all experimental methods, but is ignored by RIS theory and MC simulations of single chain. Our simulations considered both chain density and temperature expansion in polymer melt and thus our results consist with SANS-based experiments. The temperature coefficient $\kappa = d \ln \langle l_p^{(k)} \rangle / dT$ is calculated by the plateau values of persistence. In Table 1, we compare temperature coefficient κ for polymers estimated from simulation data ($l_p^{(k)}$) and normalized data (l_p^*) and comparison with reported results from literature. The effect of thermal expansion on κ is of certain extent which is much stronger for *i*PP and *i*PB-1 than PE. So the thermal expansion effect can nearly be ignored for PE. It can explain the closeness of the values from SANS and RIS, which are on the same level with our estimation. For *i*PP, the thermal expansion effect can remarkably change the temperature coefficient κ from a relative perspective. The estimation of κ from simulation data is close to zero reported by SANS, and the value from normalized data approaches the values calculated by RIS. The κ results of *i*PB are very close to *i*PP. Unfortunately, we did not find the corresponding experimental results of *i*PB.

Now an alternative approach is attempted to obtain the persistence lengths based on the single-chain structure factor, $S(q)$, [59] as defined by

$$S(q) = \frac{2}{N(N+1)} \sum_{i < j} \frac{\sin(qR_{ij})}{qR_{ij}} \quad (5)$$

where N is the number of backbone carbon atoms, q is scattering vector, and R_{ij} is the distance between the i th and j th carbon atoms.

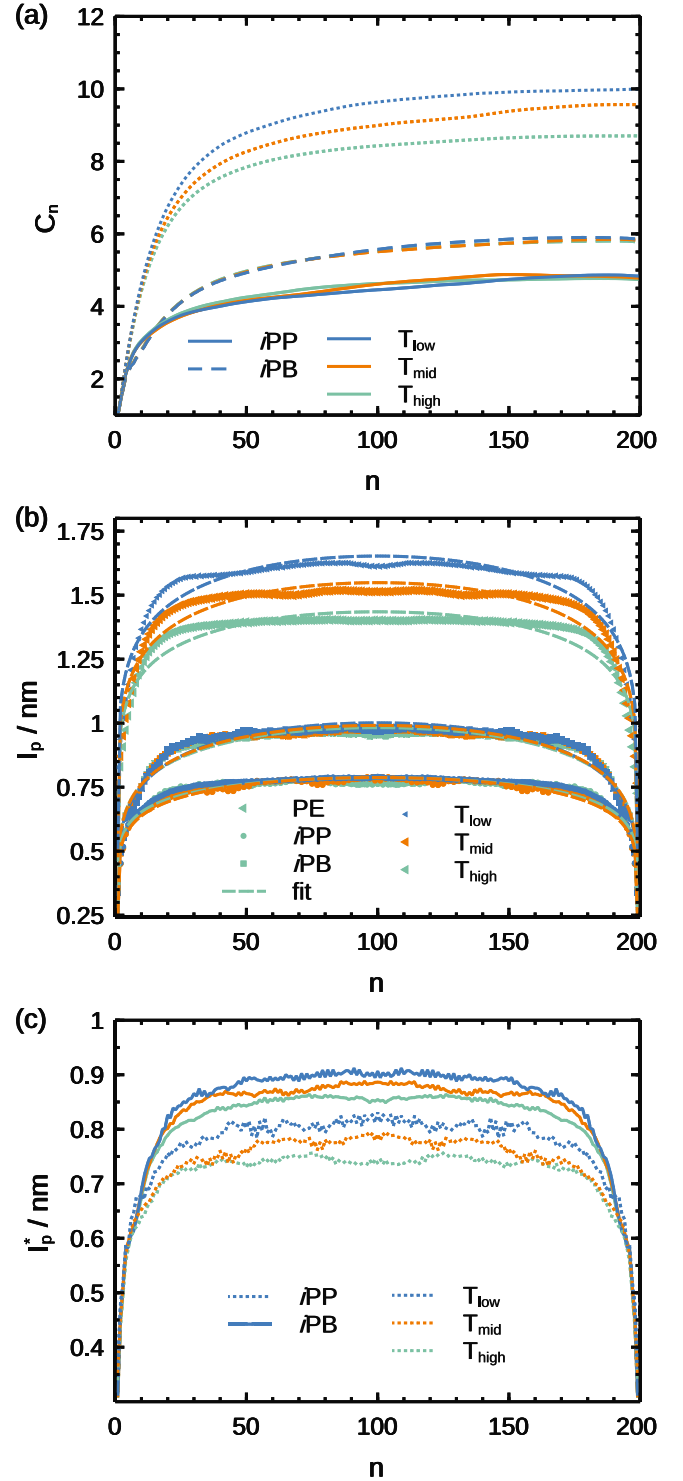


Fig. 6. (a) Flory's characteristic ratio C_n , (b) modified local persistence length $l_p^{(k)}$, and (c) normalized persistence length $l_p^{(e)}$ for PE, *i*PP, *i*PB-1 versus the number of backbone bonds n at different temperatures. The statistic noise for C_n is very high even for long time simulations. A symmetrical average processing for $l_p^{(k)}$ and $l_p^{(e)}$ is used to reduce the statistic noise.

If $N_b l_p / l_p \gg 1$ and scattering vector q is very large, namely $q l_p \gg 3$, a simple approximation is obtained:

$$N q l S(q) = \pi + \frac{2}{3} \frac{1}{q l_p} \quad (6)$$

Table 1
Temperature coefficient κ estimated from original data and normalized data.

Polymer	$\kappa \times 10^3$ (K^{-1})		SANS	RIS
	Simulation data	Normalized data		
PE	$-1.40 \pm 0.06 - 1.77 \pm 0.08$	-1.06 ± 0.07 [47]	-1.1 [58]	
<i>i</i> PP	-0.13 ± 0.07	-0.41 ± 0.02	0 [3,5]	-1.0 to -4.0 [34,36–38]
<i>i</i> PB	-0.16 ± 0.00	-0.47 ± 0.00		

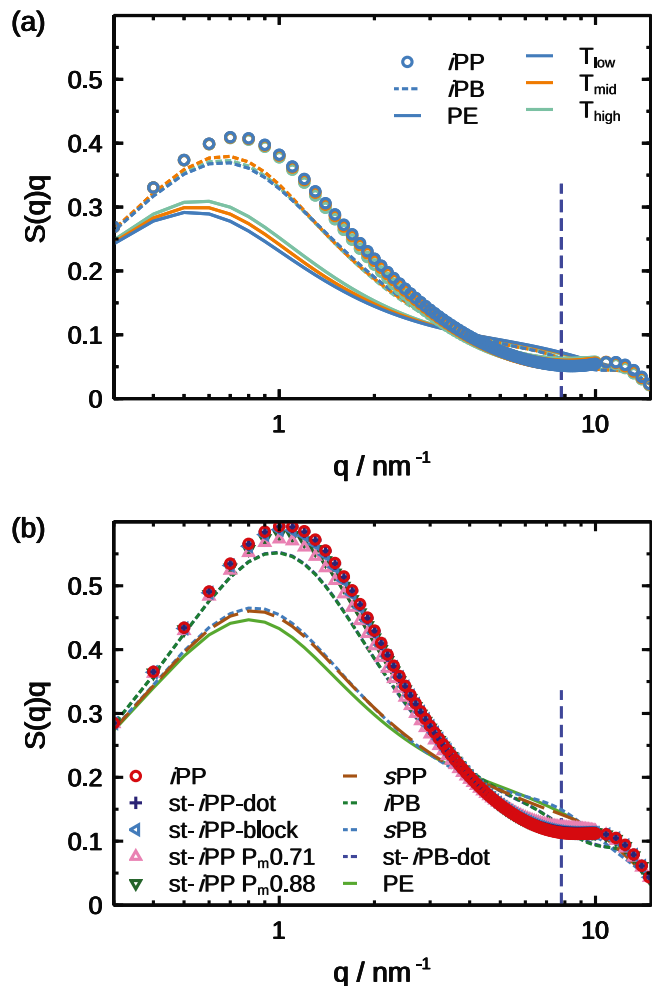


Fig. 7. The single-chain structure factor of (a) PE, *i*PP, and *i*PB-1 chains at different temperatures and (b) polymer chains shown in Fig. 2 at 600K.

This equation has been used to extract the persistence length of polymers with bottle-brush architecture. [60,61] A flat region from $q \approx l_p^{-1}$ to $q \approx l^{-1}$, the so-called ‘‘Holtzer plateau’’, is expected to see in the single-chain structure factor multiplied by q . The onset of this ‘‘Holtzer plateau’’ in q gives some information of l_p . Fig. 7(a) shows the single-chain structure factor of PE, *i*PP and *i*PB at three different temperatures as described in Fig. 6. Fig. 7(b) exhibits the single-chain structure factor of various short polymer chains with different tacticities at 600K as discussed in Fig. 2. The $S(q)q$ exhibits a ‘‘Holtzer plateau’’ only for *i*PP and st-*i*PP chains. The onset of the horizontal regions is marked by a vertical dashed line located around $q = 7.8 \text{ nm}^{-1}$. An approximate persistence length $l_p^{(k)} = 0.80 \text{ nm}$ is extracted from it, which is consistent with the estimated values from Figs. 2 and 6.

Fig. 8(a) shows the normalized distributions of dihedrals (torsion angles) along the backbone of PE, *i*PP and *i*PB-1 at different temperatures. Three torsional states, *trans* (t), *gauche plus* (g^+) and *gauche minus* (g^-) are identified by the minima of the normalized distributions of dihedrals. Specifically, the *trans* (t) state is defined as the dihedral

within $180 \pm 65^\circ$, the *gauche minus* (g^-) state from 245 to 330° , and the *gauche plus* (g^+) from 30 to 115° . All the chains have three well-defined peaks corresponding to the *trans* and two *gauche* states. The quantity of *trans* states is the largest for PE and the smallest for *i*PB-1. The quantity of *gauche* states is the smallest for PE, while the other two are close to each other. The probability of *trans* states for PE and *i*PP increases as the temperature decreases. There is little change of *trans* probability of *i*PB-1 at different temperatures.

Fig. 8(b) presents the proportion of helical segments with different length n_h in expression of dihedral number at different temperatures for *i*PP and *i*PB-1. Here the helical segments are defined based on the helical units, such as tg^+ , tg^- , g^+t , and g^-t . Each helical segment consists of the same *gauche* states, that is, sequences like tg^+tg^- are not considered. The proportion of helical segments decreases with increasing helical length. Long helices are not easy to form and stabilize in the melt. As temperature is increased, the proportion of helical segments decreases, which is more obvious for longer helical segments.

From previous results shown in Fig. 6(b), PE is much stiffer than *i*PP, while *i*PP is slightly more flexible than *i*PB-1. For *i*PP, the introduction of methyl side groups on PE results in the formation of large amounts of helices (Fig. 7), which attributes to an enhanced flexibility. For *i*PB-1, the addition of larger ethyl side groups can also lead to the formation of helices similarly. But the quantity of helices with different length is slightly higher for *i*PP than *i*PB-1, which makes *i*PP more flexible. Besides the existence of helical structures, the role of side group sizes should also be considered. Both of the steric hindrance and the excluded volume of the side groups cause an increase of persistence length. It is worth noting that similar observation about the influence of side chains on the stiffness of polymers has been reported in the literature. It mentioned that the persistence length could be systematically increased by increasing the size of side groups under good solvent conditions, and the backbone stiffness of polymers is determined by a balance between the backbone conformations and the size of the side chain. [21]

The bond orientational correlation function of *i*PP and *i*PB-1 is calculated in the next step using equation defined by:

$$\langle \cos \theta(s) \rangle = \langle \vec{r}_i \cdot \vec{r}_j \rangle / l \quad (7)$$

where \vec{r}_i is the i th bond vector along the backbone, $s = |i - j|$, and θ is the angle between two bonds separated by s bonds. Fig. 9 shows the bond orientational correlation function $\langle \cos \theta(s) \rangle$ of *i*PP and *i*PB-1 versus s in the log–log form at different temperatures. The result shows a power-law, rather than an exponential, decay of the bond orientational correlation function, especially at the middle s range. The power-law fitting curves of $\langle \cos \theta(s) \rangle = 1.00s^{-1.52}$ for *i*PP and $\langle \cos \theta(s) \rangle = 1.00s^{-1.27}$ for *i*PB are plotted as green solid and red dashed lines. Similar results have been reported in the previous works, in which bond orientational correlation functions show a power law decay rather than an exponential decay for both dense melts and at Θ point. [62–64] The inset shows the bond orientational correlation function $\langle \cos \theta(s) \rangle$ in the log-linear form within a short range at different temperatures. No obvious difference between each temperature is observed within two separated bonds ($s \leq 2$) due to the same bond angle. However, we can observe a strong oscillation at the range of $s \geq 5$ for both chains. The extent of oscillation becomes weaker for *i*PP, but not change much for *i*PB-1 when temperature is increased. This indicates that helical conformations are considerably formed in the melt of *i*PP and *i*PB-1.

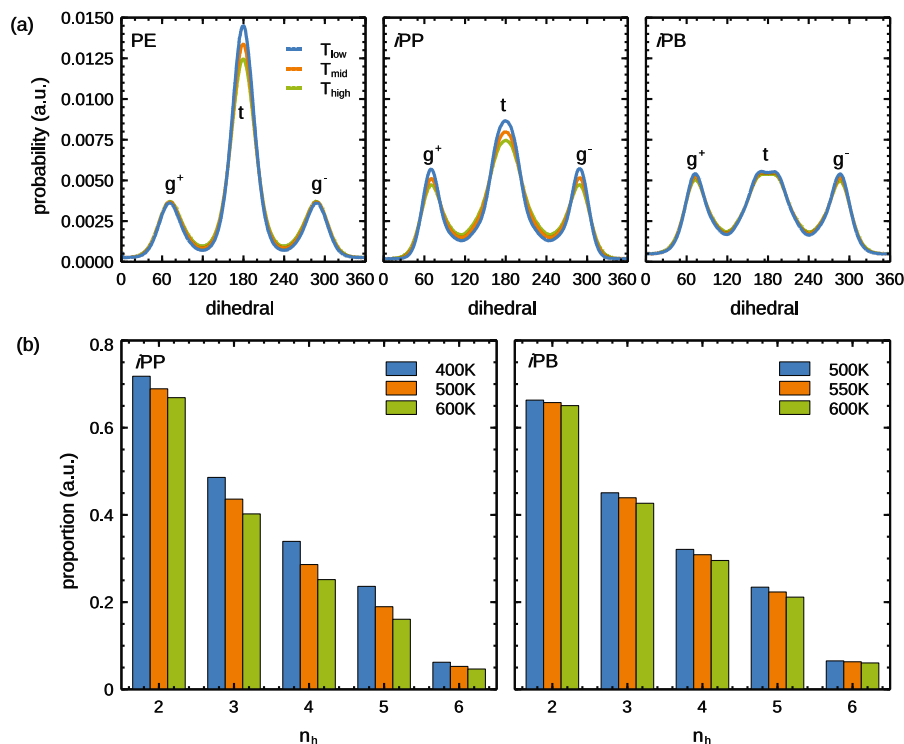


Fig. 8. (a) Normalized distributions of dihedrals along the backbone of PE, *i*PP, and *i*PB-1 at different temperatures. (b) Proportion of helical segments in different segment lengths n_h (represented with dihedral number) at different temperatures for *i*PP and *i*PB-1.

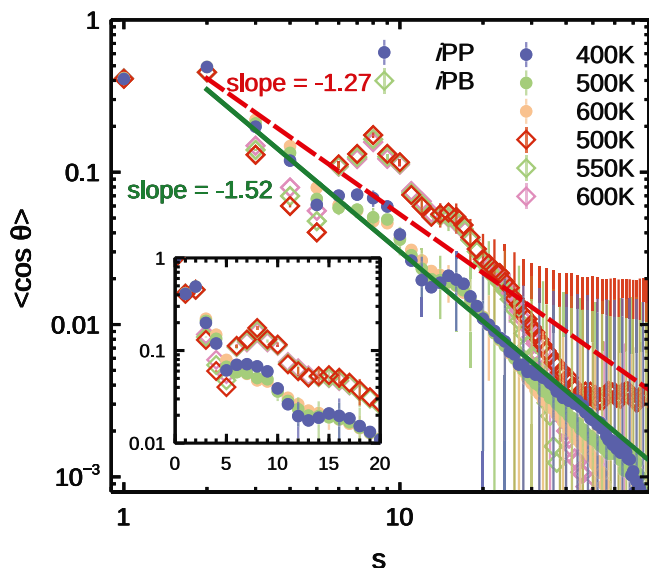


Fig. 9. Bond orientational correlation function $\langle \cos \theta(s) \rangle$ of *i*PP and *i*PB-1 versus s in the log-log form and the corresponding log-linear form in the inset.

Finally, it is necessary to rethink the standard definitions of chain stiffness, such as Flory's character ratio C_n and persistent length $l_p^{(k)}$ discussed above. We must note that these standard definitions of chain stiffness are based on coarse-grained concepts and ignore the details of local structures. As pointed by Hsu *et al* [61], standard definitions of persistence length do not describe the local "intrinsic" stiffness of real polymer chains. Here, we further emphasize the effect of detailed local structures on the chain stiffness, such as helical structures. Helical structures lead to correlation along chain backbone, which breaks the preconditions of standard methods. For an extreme example, the

correlation length in the perfect 3/1 helix is expected as infinity. Considering that helical structures are common in real polymers, a refreshed definition of chain stiffness based on all-atom concepts, rather than coarse-grained, is demanded in future studies.

4. Conclusions

In the present study, the effect of asymmetric chirality and chain density on the chain stiffness of polymers in melts is investigated by using all-atom molecular dynamics simulations. It is found that the chain stiffness of stereodeficient *i*PP and *i*PB-1, expressed by the modified local persistence length, increases significantly at the position of the polymer chain where an asymmetric stereoregular pair is introduced. Analyses of dihedral-pair distributions show that the enhanced stiffness is induced by the conformational sequences of helices with opposite chirality joined by all-*trans* series. Further it is concluded that the free energy landscape of adjacent dihedral pairs explain the various stiffness of chains with different tacticities. The temperature dependence of the chain stiffness of PE, *i*PP, and *i*PB-1 is studied, and it is revealed that the characteristic ratio and the modified local persistence length are almost independent of temperature for *i*PP and *i*PB-1. This is in line with the SANS-based measurements while contradicts with the RIS predictions. By considering the effect of chain density, the normalized persistence length decrease as temperature is increased, which is qualitatively consistent with RIS results. Thus it can be concluded that SANS-based measurements and RIS prediction are harmonic. The discrepancy between original RIS theory and SANS-based experiments is caused by the chain density which is ignored in original RIS theory and previously reported single-chain simulations. PE chain is much stiffer than *i*PP and *i*PB-1 chains, while *i*PP is slightly more flexible than that of *i*PB-1. With introduction of methyl or ethyl side groups, a large amount of helical structures are formed, which leads to enhanced chain flexibility. Comparing between *i*PP and *i*PB-1, it is known that sizes of side groups play an important role in chain stiffness. Both of the steric hindrance and the excluded volume of side groups cause an increase of persistence length, which results in a stiffer chain for *i*PB-1 than *i*PP.

List of Symbols

C_n	Flory's characteristic ratio
$l_p^{(k)}$	Modified local persistence length
l_p^*	Normalized local persistence length
κ	Temperature coefficient of chain dimensions and chain stiffness
P_m	Fractions of <i>meso</i> dyads
R	End-to-end distance of each chain
\vec{R}	End-to-end distance vector of each chain
R_{ij}	Distance between the <i>i</i> th and <i>j</i> th carbon atoms
\vec{r}_k	Unit vector of the <i>k</i> th bond along the backbone
l	Bond length
N_b	Total number of monomers
F	Equivalent free energy landscape
S	Single-chain structure factor
T	Temperature
v	Volume of polymer melt

CRediT authorship contribution statement

Ran Chen: Simulation, Data analyzing, Writing - original draft.
Chuanfu Luo: Conceptualization, Methodology, Writing - review & editing.

Declaration of competing interest

The authors declare that they have no known competing financial interests or personal relationships that could have appeared to influence the work reported in this paper.

Acknowledgments

The authors acknowledge the financial support from the National Natural Science Foundation of China (No. 21873093).

Appendix A. Supplementary data

Supplementary material related to this article can be found online at <https://doi.org/10.1016/j.commatsci.2021.111071>.

References

- [1] Z.-G. Wang, *50th anniversary perspective: Polymer conformation—A pedagogical review*, *Macromolecules* 50 (23) (2017) 9073–9114.
- [2] L.J. Fetters, W.W. Graessley, R. Krishnamoorti, D.J. Lohse, Melt chain dimensions of poly(ethylene-1-butene) copolymers via small angle neutron scattering, *Macromolecules* 30 (17) (1997) 4973–4977.
- [3] D. Ballard, P. Cheshire, G. Longman, J. Schelten, Small-angle neutron scattering studies of isotropic polypropylene, *Polymer* 19 (4) (1978) 379–385.
- [4] G.D. Smith, D.Y. Yoon, R.L. Jaffe, R.H. Colby, R. Krishnamoorti, L.J. Fetters, Conformations and structures of poly(oxyethylene) melts from molecular dynamics simulations and small-angle neutron scattering experiments, *Macromolecules* 29 (10) (1996) 3462–3469.
- [5] A. Zirkel, V. Urban, D. Richter, L.J. Fetters, J.S. Huang, R. Kampmann, N. Hadjichristidis, Small-angle neutron scattering evaluation of the temperature dependence of atactic polypropylene and poly(1-butene) chain dimensions in the melt, *Macromolecules* 25 (23) (1992) 6148–6155.
- [6] R. Krishnamoorti, W.W. Graessley, A. Zirkel, D. Richter, N. Hadjichristidis, L.J. Fetters, D.J. Lohse, Melt-state polymer chain dimensions as a function of temperature, *J. Polym. Sci. B* 40 (16) (2002) 1768–1776.
- [7] Z. Xu, N. Hadjichristidis, J.M. Carella, L.J. Fetters, Characteristic ratios of atactic poly(vinylethylene) and poly(ethyleneethylene), *Macromolecules* 16 (6) (1983) 925–929.
- [8] J.W. Mays, L.J. Fetters, Temperature coefficients of unperturbed dimensions for atactic polypropylene and alternating poly(ethylene-propylene), *Macromolecules* 22 (2) (1989) 921–926.
- [9] L.J. Fetters, D.J. Lohse, D. Richter, T.A. Witten, A. Zirkel, Connection between polymer molecular weight, density, chain dimensions, and melt viscoelastic properties, *Macromolecules* 27 (17) (1994) 4639–4647.
- [10] P.J. Flory, Foundations of rotational isomeric state theory and general methods for generating configurational averages, *Macromolecules* 7 (3) (1974) 381–392.
- [11] G.C. Rutledge, Conformational theory of large molecules: The rotational isomeric state model in macromolecular systems, *AIChE J.* 42 (4) (1996) 1199–1200.
- [12] Z. Zhou, W. Yang, D. Yan, H. Liu, Temperature dependence of polypropylene configurations: Temperature dependence of polypropylene configurations, *Macromol. Theory Simul.* 23 (2) (2014) 76–83.
- [13] D.N. Theodorou, U.W. Suter, Shape of unperturbed linear polymers: Polypropylene, *Macromolecules* 18 (6) (1985) 1206–1214.
- [14] U.W. Suter, P.J. Flory, Conformational energy and configurational statistics of polypropylene, *Macromolecules* 8 (6) (1975) 765–776.
- [15] U. Biskup, H.-J. Cantow, Calculations on the unperturbed dimensions of polypropylenes, *Macromolecules* 5 (5) (1972) 546–550.
- [16] P.-N. Tzounis, D.V. Argyropoulou, S.D. Anogiannakis, D.N. Theodorou, Tacticity effect on the conformational properties of polypropylene and poly(ethylene-propylene) copolymers, *Macromolecules* 51 (17) (2018) 6878–6891.
- [17] P.-N. Tzounis, S.D. Anogiannakis, D.N. Theodorou, General methodology for estimating the stiffness of polymer chains from their chemical constitution: A single unperturbed chain Monte Carlo algorithm, *Macromolecules* 50 (11) (2017) 4575–4587.
- [18] K. Moorthi, K. Kamio, J. Ramos, D.N. Theodorou, Monte Carlo simulation of short chain branched polyolefins: Structure and properties, *Macromolecules* 45 (20) (2012) 8453–8466.
- [19] S.J. Antoniadis, C.T. Samara, D.N. Theodorou, Molecular dynamics of atactic polypropylene melts, *Macromolecules* 31 (22) (1998) 7944–7952.
- [20] S.J. Antoniadis, C.T. Samara, D.N. Theodorou, Effect of tacticity on the molecular dynamics of polypropylene melts, *Macromolecules* 32 (25) (1999) 8635–8644.
- [21] J. Wescott, S. Hanna, The influence of flexible side chains on the dimensions of flexible polymers, *Comput. Theor. Polymer. Sci.* 9 (3) (1999) 307–326.
- [22] A. De Nicola, G. Munaó, N. Grizzuti, F. Auremma, C. De Rosa, A. Sevinck, G. Milano, Generation of well relaxed all atom models of stereoregular polymers: A validation of hybrid particle-field molecular dynamics for polypropylene melts of different tacticities, *Soft Mater.* (2020) 1–14.
- [23] J. Honeycutt, A general simulation method for computing conformational properties of single polymer chains, *Comput. Theor. Polymer. Sci.* 8 (1) (1998) 1–8.
- [24] V. Subramanian, P. Samuel Asirvatham, R. Balakrishnan, T. Ramasami, Molecular mechanics studies on polypropylene and polymethylmethacrylate polymers, *Chem. Phys. Lett.* 342 (5) (2001) 603–609.
- [25] A. Eckstein, C. Friedrich, A. Lobbrecht, R. Spitz, R. Mühlaupt, Comparison of the viscoelastic properties of syndio- and isotactic polypropylenes, *Acta Polym.* 48 (12) (1997) 41–46.
- [26] A. Eckstein, J. Suhm, C. Friedrich, R.-D. Maier, J. Sassmannshausen, M. Bochmann, R. Mühlaupt, Determination of plateau moduli and entanglement molecular weights of isotactic, syndiotactic, and atactic polypropylenes synthesized with metallocene catalysts, *Macromolecules* 31 (4) (1998) 1335–1340.
- [27] L.J. Fetters, D.J. Lohse, C.A. García-Franco, P. Brant, D. Richter, Prediction of melt state poly(α -olefin) rheological properties: The unsuspected role of the average molecular weight per backbone bond, *Macromolecules* 35 (27) (2002) 10096–10101.
- [28] T.D. Jones, K.A. Chaffin, F.S. Bates, B.K. Annis, E.W. Hagaman, M.-H. Kim, G.D. Wignall, W. Fan, R. Waymouth, Effect of tacticity on coil dimensions and thermodynamic properties of polypropylene, *Macromolecules* 35 (13) (2002) 5061–5068.
- [29] C. De Rosa, F. Auremma, O. Ruiz de Ballesteros, The role of crystals in the elasticity of semicrystalline thermoplastic elastomers, *Chem. Mater.* 18 (15) (2006) 3523–3530.
- [30] C. Derosa, F. Auremma, Structure and physical properties of syndiotactic polypropylene: A highly crystalline thermoplastic elastomer, *Prog. Polym. Sci.* 31 (2) (2006) 145–237.
- [31] M. Destrée, F. Lauprêtre, A. Lyulin, J.-P. Ryckaert, Local dynamics of isotactic and syndiotactic polypropylene in solution, *J. Chem. Phys.* 112 (21) (2000) 9632–9644.
- [32] C. Liu, J. Yu, J. He, W. Liu, C. Sun, Z. Jing, A reexamination of and M_e of syndiotactic polypropylenes with metallocene catalysts, *Macromolecules* 37 (24) (2004) 9279–9282.
- [33] T. Pinijmontree, P. Choi, V. Vao-soongnern, Effect of stereochemical sequence on the dynamics of atactic polypropylene melt, *Macromol. Res.* 22 (2) (2014) 187–193.
- [34] R.H. Boyd, S.M. Breittling, Conformational properties of polypropylene, *Macromolecules* 5 (3) (1972) 279–286.
- [35] C. Liu, P. Liu, Q. Chen, B. Du, Z. Wang, Entanglement relaxation of poly(1-butene) and its copolymer with ethylene detected in conventional shear rheometer and quartz resonator, *J. Rheol.* 63 (1) (2019) 167–177.
- [36] J.E. Mark, On the configurational statistics of ethylene-propylene copolymers, *J. Chem. Phys.* 57 (6) (1972) 2541–2548.
- [37] G. Allegra, M. Calligaris, L. Randaccio, G. Moraglio, Isotactic polypropylene. Unperturbed dimensions calculated accounting for all skeletal rotations, *Macromolecules* 6 (3) (1973) 397–403.
- [38] H. Wittwer, U.W. Suter, Conformational characteristics of poly(1-alkenes). Flexible side groups and the limits of simple rotational isomeric state models, *Macromolecules* 18 (3) (1985) 403–411.

- [39] J.B. Kinsinger, R.E. Hughes, The unperturbed dimensions of atactic and isotactic polypropylene, *J. Phys. Chem.* 67 (9) (1963) 1922–1923.
- [40] A. Nakajima, A. Saijyo, Unperturbed chain dimensions of isotactic polypropylene in theta solvents, *J. Polym. Sci. A-2 Polym. Phys.* 6 (4) (1968) 735–744.
- [41] G. Moraglio, G. Gianotti, U. Bonicelli, Unperturbed dimensions of isotactic and atactic polypropylene at various temperatures, *Eur. Polym. J.* 9 (7) (1973) 623–630.
- [42] A. Zirkel, D. Richter, L.J. Fetters, D. Schneider, V. Graciano, N. Hadjichristidis, A SANS-based evaluation of the chain dimension temperature dependence of poly(ethylene) under .THETA.-conditions, *Macromolecules* 28 (15) (1995) 5262–5266.
- [43] N. Kuwahara, S. Saeki, S. Konno, M. Kaneko, Temperature dependence of polymer chain dimensions in the polystyrene-cyclopentane system, *Polymer* 15 (2) (1974) 66–68.
- [44] J.W. Mays, N. Hadjichristidis, L.J. Fetters, Solvent and temperature influences on polystyrene unperturbed dimensions, *Macromolecules* 18 (11) (1985) 2231–2236.
- [45] A.T. Boothroyd, A.R. Rennie, G.D. Wignall, Temperature coefficients for the chain dimensions of polystyrene and polymethylmethacrylate, *J. Chem. Phys.* 99 (11) (1993) 9135–9144.
- [46] R. Chiang, Intrinsic viscosity-molecular weight relationship for fractions of linear polyethylene, *J. Phys. Chem.* 69 (5) (1965) 1645–1653.
- [47] A.T. Boothroyd, A.R. Rennie, C.B. Boothroyd, Direct measurement of the temperature dependence of the unperturbed dimensions of a polymer, *Europhys. Lett.* 15 (7) (1991) 715–719.
- [48] B. Hess, C. Kutzner, D. van der Spoel, E. Lindahl, GROMACS 4: Algorithms for highly efficient, load-balanced, and scalable molecular simulation, *J. Chem. Theory Comput.* 4 (3) (2008) 435–447.
- [49] W.L. Jorgensen, J.D. Madura, C.J. Swenson, Optimized intermolecular potential functions for liquid hydrocarbons, *J. Am. Chem. Soc.* 106 (22) (1984) 6638–6646.
- [50] W.L. Jorgensen, J. Tirado-Rives, The OPLS (optimized potentials for liquid simulations) potential functions for proteins, energy minimizations for crystals of cyclic peptides and crambin, *J. Am. Chem. Soc.* 110 (6) (1988) 1657–1666.
- [51] R. Connolly, G. Bellesia, E.G. Timoshenko, Y.A. Kuznetsov, S. Elli, F. Ganazzoli, “Intrinsic” and “Topological” stiffness in branched polymers, *Macromolecules* 38 (12) (2005) 5288–5299.
- [52] S. Elli, F. Ganazzoli, E.G. Timoshenko, Y.A. Kuznetsov, R. Connolly, Size and persistence length of molecular bottle-brushes by Monte Carlo simulations, *J. Chem. Phys.* 120 (13) (2004) 6257–6267.
- [53] A. Yethiraj, A Monte Carlo simulation study of branched polymers, *J. Chem. Phys.* 125 (20) (2006) 204901.
- [54] N. Ahmad, R. Di Girolamo, F. Auriemma, C. De Rosa, N. Grizzuti, Relations between stereoregularity and melt viscoelasticity of syndiotactic polypropylene, *Macromolecules* 46 (19) (2013) 7940–7946.
- [55] S. Brückner, G. Allegra, P. Corradini, Helix inversions in polypropylene and polystyrene, *Macromolecules* 35 (10) (2002) 3928–3936.
- [56] L. Schäfer, A. Ostendorf, J. Hager, Scaling of the correlations among segment directions of a self-repelling polymer chain, *J. Phys. A: Math. Gen.* 32 (45) (1999) 7875–7899.
- [57] L. Schäfer, K. Elsner, Calculation of the persistence length of a flexible polymer chain with short-range self-repulsion, *Eur. Phys. J. E* 13 (3) (2004) 225–237.
- [58] A. Abe, R.L. Jernigan, P.J. Flory, Conformational energies of N-alkanes and the random configuration of higher homologs including polymethylene, *J. Am. Chem. Soc.* 88 (4) (1966) 631–639.
- [59] G. Strobl, *The Physics of Polymers*, second ed., Springer, Berlin, Heidelberg, ISBN: 978-3-540-25278-8, 2007.
- [60] S. Lecommandoux, F. Chécot, R. Borsali, M. Schappacher, A. Deffieux, A. Brlet, J.P. Cotton, Effect of dense grafting on the backbone conformation of bottlebrush polymers: Determination of the persistence length in solution, *Macromolecules* 35 (23) (2002) 8878–8881.
- [61] H.-P. Hsu, W. Paul, K. Binder, Standard definitions of persistence length do not describe the local “Intrinsic” stiffness of real polymer chains, *Macromolecules* 43 (6) (2010) 3094–3102.
- [62] J.P. Wittmer, H. Meyer, J. Baschnagel, A. Johner, S. Obukhov, L. Mattioni, M. Müller, A.N. Semenov, Long range bond-bond correlations in dense polymer solutions, *Phys. Rev. Lett.* 93 (14) (2004) 147801.
- [63] J.P. Wittmer, P. Beckrich, H. Meyer, A. Cavallo, A. Johner, J. Baschnagel, Intramolecular long-range correlations in polymer melts: The segmental size distribution and its moments, *Phys. Rev. E* 76 (1) (2007) 011803.
- [64] D. Shirvanyants, S. Panyukov, Q. Liao, M. Rubinstein, Long-range correlations in a polymer chain due to its connectivity, *Macromolecules* 41 (4) (2008) 1475–1485.